A Theory for Midlatitude Forcing of Tropical Motions during Winter Monsoons

HOCK LIM[1] AND C.-P. CHANG

Department of Meteorology, Naval Postgraduate School, Monterey, CA 93940

(Manuscript received 31 March 1981, in final form 29 June 1981)

ABSTRACT

In order to understand the northeasterly monsoon surges and associated tropical motions over Southeast Asia during northern winter, the dynamic response of the tropical atmosphere to midlatitude pressure surges is studied using the linearized shallow-water equations on an equatorial β plane. The forcing is specified to have a Gaussian spatial distribution with a zonal scale corresponding to approximately wavenumber 7 and a meridional scale of approximately 11°. It rises rapidly from zero to maximum within one day or less and then decays slowly over 2–4 days. The main results are as follows:

1) After an initial period of gravity-wave type motions with strong northerly winds, the main tropical response takes the form of a Rossby wave group.
2) A pronounced northeast–southwest tilt in this Rossby wave group develops due to the faster westward group velocity of the lower meridional modes relative to the higher meridional modes.
3) Several conspicuous features of the Rossby response closely resemble the observed flow pattern of the northeast monsoon region, notably the northeasterly wind streak over the South China Sea during cold surges, the mean winter condition of a cyclonic shear trough extending from Borneo to the Philippines, and the enhancement of cyclonic circulation near the northern Borneo coast after surges.
4) The pressure surge forcing also gives rise to eastward moving wave groups of the Kelvin, mixed Rossby–gravity, and inertia–gravity (mainly $n = 0$) modes. The Kelvin wave response, as in the case of thermally forced Kelvin waves, has a preference for longer wavelengths. These wave groups offer a possible interpretation for the eastward moving cloud patterns observed during Winter MONEX by Williams (1981).

Our results suggest that the gross features of the synoptic-scale tropical motions in the northeast monsoon region can be explained in terms of simple equatorial β-plane dynamics without taking into account other physical factors such as orography or boundary-layer friction.

1. Introduction

During the northern winter, the East Asia continental region is dominated by a strong surface high over Siberia and northern China. Radiative cooling and persistent cold air advection throughout the troposphere maintain a layer of very cold air over the frozen land. The presence of the Tibetan plateau to the southwest restricts the movement of this cold air mass and contributes to the buildup of the surface high. A strong baroclinic zone exists between this cold continental air mass and the warm tropical air mass to its south. The passage of a deep upper trough in the midlatitudes often triggers intense anticyclogenesis over central China and cyclogenesis over the East China Sea (Danielsen and Ho, 1969).[2] Coupled with these changes is a downstream acceleration of the upper level jet over East Asia which is consistent dynamically with the increased surface high pressure center (Webster, 1981; Chang and Lau, 1981). As the pressure gradient across the East China coast tightens, cold air bursts out of the continent toward the South China Sea and a "cold surge" is initiated. In a normal season, cold surges may occur at intervals of several days to about two weeks.

In the midlatitudes, a surge arrives with a steep rise of surface pressure, a sharp drop of temperature and a strengthening of northerly winds. The cold front leading the surge sometimes brings stratus and rain but a strong surge is generally associated with subsiding motions which leads to clearing of weather (Danielsen and Ho, 1969[2]; Ramage, 1971). Although the front associated with a surge cannot normally be followed southward of about 25°N, the surge propagates equatorward in dramatic fashion. As a vigorous surge reaches the South China coast, northerly winds freshen almost simultaneously several hundred kilometers to the south, far beyond the region where the winds could have pushed the front

[1] Permanent affiliation: Meteorological Service Singapore, 41 Hillcrest Rd., Singapore 1128.

[2] Danielson, E. F., and F. P. Ho, 1969: An isentropic trajectory study of a strong northeast monsoon surge. Sci. Rep. No. 2, AFCRL-69-0036, Hawaii Institute of Geophysics, 13 pp.

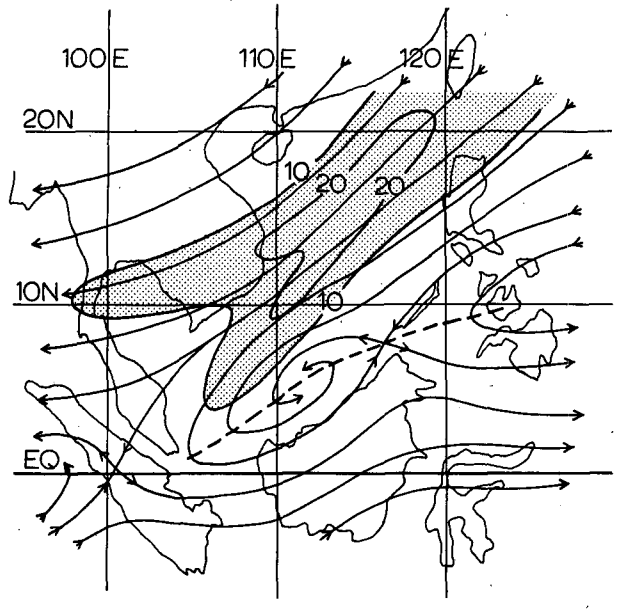

FIG. 1. A schematic diagram of surface wind field during active winter monsoon surge. The isotachs are in units of m s^{-1} and areas with larger than 10 m s^{-1} wind speed are shaded. The thick dashed-line indicates the usual position of the quasi-permanent equatorial shear line (trough) north of Borneo.

(Ramage, 1971; Chang *et al.*, 1979). A belt of strong northeasterly winds forms within 24 h off the South China and Vietnam coasts (shown schematically in Fig. 1).

In the equatorial region south of East Asia lies the "maritime continent" of Malaysia and Indonesia. During winter, extensive deep cumulus convection over this region supplies a large amount of latent heat to the atmosphere and is believed to be one of the most important energy sources that drive the winter general circulation (Ramage, 1971). In a series of observational studies, Chang *et al.* (1979) and Chang and Lau (1980, 1981) suggested that this equatorial convective heat source may interact with the cold surges from the north, resulting in modifications of both synoptic and planetary scale motions. In the synoptic scale, they found indications that a quasi-stationary cyclonic circulation system near the northern coast of Borneo and its associated cumulus convection intensify on the arrival of wind surges. This cyclonic circulation is embedded in an eastnortheast–westsouthwest oriented equatorial trough (Bryant, 1958). Its convective activity appears to contribute significantly to the total heat source of the maritime continent. In the planetary scale, they found a steady increase of divergent outflow over the maritime continent in the upper atmosphere following the onset of a surge. This divergent outflow, which probably is the consequence of enhanced organized convection, appears to spread both eastward and westward, resulting in strengthened Walker circulations over the equatorial Pacific and the Indian Oceans.

In another recent study, Williams (1981) showed a case of cross-equatorial influence of the northeasterly surge. About three days after a surge crossed the South China coast, he observed a slow pressure rise over western Indonesia. As if accelerated by the east–west pressure gradient, westerly winds strengthened and convective systems were observed to develop in the southern equatorial region and drift eastward at a speed of 10 m s^{-1}.

Although much remains to be learned about the winter monsoon surges, observational studies mentioned above suggest that they may play an important part in the various midlatitude, tropical, interhemispherical and longitudinal interactions. The purpose of this paper is to carry out a theoretical study of the effects of the surges in the tropics in terms of the basic dynamics of laterally forced tropical motions. We shall leave aside such questions as the cause of the intense anticyclogenesis in the midlatitudes that initiates a surge and just concentrate on the dynamical response of the tropical atmosphere to such a midlatitude development. A localized transient mass source will be used to simulate the intense anticyclogenesis, and the tropical response will be studied using the linearized β-plane shallow-water equations.

The use of the shallow water equations may be subject to criticisms as the tropical motions responding to surges are likely to be associated with cumulus convection. However, the shallow-water system may be regarded as a two-level approximation to a baroclinic system because, when not considering the effects of friction, the two are equivalent for a given vertical structure (Matsuno, 1966). We shall take such a view in this study and choose a scale height for the shallow water model such that the model waves have phase speeds close to those observed. This approximation is justified because Chang (1977) has shown that in a baroclinic model, cumulus friction alters the equatorial wave behavior in such a way that the vertical wavelength of even the low-frequency waves tends to be comparable to the depth of the troposphere.

2. Equations and solutions

The linearized shallow-water equations with a motionless basic state on a β plane are

$$\left.\begin{aligned} &\frac{\partial u'}{\partial t} + g\frac{\partial h'}{\partial x} - \beta y v' = 0 \\ &\frac{\partial v'}{\partial t} + g\frac{\partial h'}{\partial y} + \beta y u' = 0 \\ &\frac{\partial h'}{\partial t} + H\left(\frac{\partial u'}{\partial x} + \frac{\partial v'}{\partial y}\right) = \Phi' \end{aligned}\right\}. \qquad (1)$$

The symbols used in this study are defined in Appendix A. Motions are forced by the inhomogeneous

term Φ'. This term represents a mass source which will be specified in an appropriate form to simulate the midlatitude anticyclogenesis observed before a surge. According to Matsuno (1966), we expect the solutions of (1) to consist of, besides transients and zonally symmetric modes, Rossby waves, mixed Rossby–gravity waves, inertia–gravity waves and Kelvin waves.

Expanding the variables in terms of a Fourier series

$$\xi' = \sum_{m=0}^{\infty} \left[\xi_c'(m, y, t) \cos \frac{2\pi m}{L} x + \xi_s'(m, y, t) \sin \frac{2\pi m}{L} x \right],$$

and carrying out a Fourier transform in time, we obtain the following equation for the meridional velocity

$$\frac{\partial^2 v^T}{\partial \zeta^2} + \left(\frac{\omega^3 - k^2c^2\omega - kc^2\beta}{\beta c \omega} - \zeta^2 \right) v^T = \frac{g}{(\beta c)^{1/2}} \left(\frac{\zeta k}{\omega} \Phi^T + \frac{1}{c} \frac{\partial \Phi^T}{\partial \zeta} \right). \quad (2)$$

To represent a pressure surge, we let

$$\Phi' = \left\{ \begin{array}{ll} \sum_{m=0}^{\infty} [\Phi_c(m, \zeta) \cos kx + \Phi_s(m, \zeta) \sin kx] \frac{t^2}{2\tau^3} e^{-t/\tau} & \text{for } t \geq 0 \\ 0 & \text{for } t < 0 \end{array} \right\}. \quad (3)$$

This form allows us flexibility to specify the spatial and temperal scales of the forcing. The time-dependent part of (3) is normalized in the sense that a total time integration gives a constant value of unity. Eq. (2) may now be written as

$$\frac{\partial^2 v^T}{\partial \zeta^2} + \left(\frac{\omega^3 - k^2c^2\omega - \beta kc^2}{\beta c \omega} - \zeta^2 \right) v^T = \frac{g}{(\beta c)^{1/2}} \left(\frac{\zeta k}{\omega} \Phi^* + \frac{1}{c} \frac{\partial \Phi^*}{\partial \zeta} \right) \frac{1}{(1 + i\omega\tau)^3}. \quad (4)$$

Considering only variables which vanish as $|y| \to \infty$, we may expand them in terms of the Hermite functions

$$\Phi^* = \sum_{n=0}^{\infty} \Phi_n D_n(\zeta), \quad \zeta^T = \sum_{n=0}^{\infty} \xi_n D_n(\zeta).$$

The equation for the coefficients of expansion v_n is

$$v_n = \frac{g(\beta c)^{1/2} \left\{ k[(n+1)\Phi_{n+1} + \tfrac{1}{2}\Phi_{n-1}] + \frac{\omega}{c}[(n+1)\Phi_{n+1} - \tfrac{1}{2}\Phi_{n-1}] \right\}}{(\omega - \omega_{n0})(\omega - \omega_{n1})(\omega - \omega_{n2})(1 + i\tau\omega)^3}, \quad (5)$$

where ω_{n0}, ω_{n1}, ω_{n2} are the three real roots of the following equation:

$$\omega^3 - [k^2c^2 + (2n+1)\beta c]\omega - \beta kc^2 = 0. \quad (6)$$

For $n > 0$, the three roots fall within the intervals

$$(-\infty, -kc), \ (-kc, 0) \text{ and } (kc, \infty).$$

However, when $n = 0$, one of the two negative roots, say, ω_{n1}, becomes equal to $-kc$ and in (5) the factor $(\omega - \omega_{n1})$ in the denominator cancels off with the factor $(k + \omega/c)$ in the numerator, giving the following equation for v_0:

$$v_0 = \frac{g(\beta/c)^{1/2}\Phi_1}{(\omega - \omega_{00})(\omega - \omega_{02})(1 + i\tau\omega)^3}. \quad (7)$$

The solution for v' may now be obtained by a term-by-term inverse Fourier transform of the expansion $v^T = \sum_{n=0}^{\infty} v_n D_n$. The inverse transforms may be carried out with the help of the calculus of residues. There are four singularities in v_n (but only three in v_0). The contour of integration may be indented at the real singularities ω_{ni} as shown in Fig. 2. For $t < 0$, the contour of integration may be closed by a semicircle in the lower ω_r-ω_i plane. Since the contour of integration encloses no singularity, the solution is $v' = 0$.

For $t > 0$, the contour of integration must be closed with a semicircle in the upper ω_r-ω_i plane

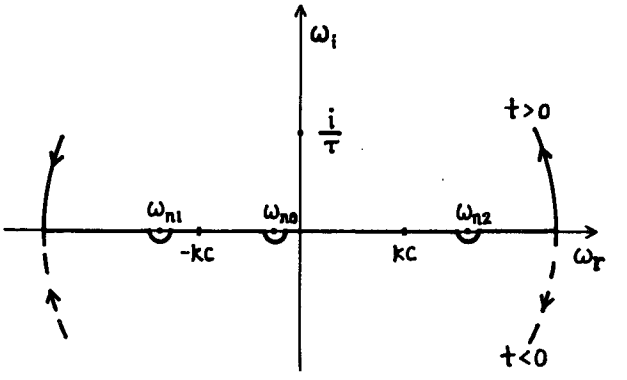

FIG. 2. Contour of integration for inverse transformation of Eqs. (5) and (7). Singularities of the integrands are i/τ, ω_{n0}, ω_{n1} and ω_{n2}.

and the solution obtained consists of three components: a transient motion excited by the forcing (identified by the presence of the exponential factor $e^{-t/\tau}$) which is contributed by the residue at the singularity i/τ; Rossby waves contributed by the residues at the singularities ω_{n0} and inertia–gravity waves by those at ω_{n1} and ω_{n2}. In the case of $n = 0$, the root ω_{01} does not give rise to a singularity and therefore does not contribute to the final solution. The singularity ω_{02} gives rise to an eastward propagating inertia–gravity wave while the singularity ω_{00} to a westward propagating mixed Rossby–gravity wave.

The equations for u^T and h^T are

$$u^T = \frac{-igk\Phi_0 D_0}{(1 + i\tau\omega)^3(\omega - kc)(\omega + kc)} + \frac{-ig\beta\Phi_1 D_1}{2(\omega - \omega_{00})(\omega - \omega_{02})(1 + i\tau\omega)^3(\omega - kc)}$$
$$+ \sum_{n=1}^{\infty} \left\{ \frac{-igk\Phi_n D_n}{(1 + i\tau\omega)^3(\omega + kc)(\omega - kc)} + \frac{-ig\beta[n(n+1)\Phi_{n+1}D_{n-1} - \Phi_{n-1}D_{n+1}/4]}{(\omega - \omega_{n0})(\omega - \omega_{n1})(\omega - \omega_{n2})(1 + i\tau\omega)^3} \right.$$
$$+ \frac{-ig\beta(n+1)\Phi_{n+1}D_{n+1}(\omega + kc)}{2(\omega - \omega_{n0})(\omega - \omega_{n1})(\omega - \omega_{n2})(1 + i\tau\omega)^3(\omega - kc)}$$
$$\left. + \frac{ign\Phi_{n-1}D_{n-1}(\omega - kc)\beta}{2(\omega - \omega_{n0})(\omega - \omega_{n1})(\omega - \omega_{n2})(1 + i\tau\omega)^3(\omega + kc)} \right\}, \quad (8)$$

and

$$h^T = \sum_{n=0}^{\infty} \frac{-i\omega\Phi_n D_n}{(1 + i\omega\tau)^3(\omega - kc)(\omega + kc)} - \frac{i\beta c\Phi_1 D_1}{2(\omega - \omega_{00})(\omega - \omega_{02})(1 + i\tau\omega)^3(\omega - kc)}$$
$$+ \sum_{n=1}^{\infty} \frac{i\beta c[n(n+1)\Phi_{n+1}D_{n-1} + \Phi_{n-1}D_{n+1}]}{(\omega - \omega_{n0})(\omega - \omega_{n1})(\omega - \omega_{n2})(1 + i\tau\omega)^3} + \sum_{n=1}^{\infty} \frac{-i\beta c \frac{n+1}{2}(\omega + kc)\Phi_{n+1}D_{n+1}}{(\omega - \omega_{n0})(\omega - \omega_{n1})(\omega - \omega_{n2})(1 + i\tau\omega)^3(\omega - kc)}$$
$$+ \sum_{n=1}^{\infty} \frac{-i\beta c \frac{n}{2}(\omega - kc)\Phi_{n-1}D_{n-1}}{(\omega - \omega_{n0})(\omega - \omega_{n1})(\omega - \omega_{n2})(1 + i\tau\omega)^3(\omega + kc)}. \quad (9)$$

Inverse transformation of (8) and (9) may be carried out by indenting the contour of integration around the singularities on the real axis (ω_{ni} and $\pm kc$) as in the case for (5) and (7). Rossby waves, inertia–gravity waves and transients are again obtained by evaluating the residues at the singularities ω_{ni} and i/τ. In addition, the singularities $\pm kc$ contribute Kelvin waves as part of the solution. In the case $n = 0$, $\omega_{01} = -kc$ again does not contribute to the final solution while ω_{00} and ω_{02} contribute the mixed Rossby–gravity and $n = 1$ inertia–gravity waves, respectively.

The case $m = 0$ (i.e., $k = 0$) requires separate treatment. A similar procedure produces the solution of this zonal mode which consists of a stationary zonal geostrophic flow and standing waves of frequencies $\omega_n = [(2n + 1)\beta c]^{1/2}$ trapped at the equator.

The complete solutions for u', v' and h' are given in Appendix B.

3. Results

The basic equation and solutions show that a midlatitude forcing can excite Rossby waves, Kelvin waves, mixed Rossby–gravity waves and inertia–gravity waves in the tropics. The amplitude of each of these excited waves depends on many factors—the amplitude of the forcing (or more precisely, the magnitude of the appropriate coefficient in its Hermite-Fourier expansion), the time scale of the forcing τ, the frequency of the wave ω_{ni}, etc. Our results will show that, in general, forcing with large time and space scales excites mainly Rossby waves and Kelvin waves. As the time scale decreases, the amplitudes of mixed Rossby–gravity waves and inertia–gravity waves increase. The same is true as the space scale decreases (not shown).

Since no dissipative effect is considered in the theory, each of these waves propagates along at its own phase speed and maintains a constant amplitude. However, in the beginning the combined motion of all waves is masked (cancelled exactly at $t = 0$) by the transient component of the solution. But as time goes on, the transient component fades away and a description of the motion in terms of the different wave modes becomes possible and appropriate. According to the theory of dispersive linear wave motion (Lighthill, 1965), we may anticipate that the different wave modes gradually

become separated from each other and reveal themselves in a readily identifiable form at different locations according to their group velocities.

To study the tropical response to a pressure-surge forcing, three cases of large spatial scale forcing are computed. The first case shows a combined Rossby wave and Kelvin wave response to a slow time scale forcing while the second case shows pronounced mixed Rossby–gravity wave and inertia–gravity wave response to a fast time scale forcing. The last case has a forcing function that contains multiple time scales in order to show the tropical developments following a "realistic" pressure surge.

In all three cases the forcing is specified to have a Gaussian spatial distribution such that (3) becomes

$$\Phi' = \exp\left\{-\frac{1}{2}\left[\left(\frac{\zeta - a}{\sigma}\right)^2 + \left(\frac{x}{\lambda}\right)^2\right]\right\} \times \left(\frac{t^2}{2\tau^3} e^{-t/\tau}\right). \quad (10)$$

Here the ζ profile is expanded in terms of the Hermite solutions $D_n(\zeta)$,

$$\exp\left[-\frac{1}{2}\left(\frac{\zeta - a}{\sigma}\right)^2\right] = \sum_{n=0}^{\infty} p_n D_n(\zeta), \quad (11)$$

where the expansion coefficients p_n may be readily evaluated using the following recurrent relation:

$$p_n = \frac{a}{n(1+\sigma^2)} p_{n-1} + \frac{\sigma^2 - 1}{2n(1+\sigma^2)} p_{n-2}$$

with

$$p_{-1} = 0$$

and

$$p_0 = \left(\frac{2}{1+\sigma^2}\right)^{1/2} \sigma \exp\left[-\frac{a^2}{2(1+\sigma^2)}\right].$$

For all cases the spatial scale of the forcing is set by specifying $\sigma = 1$ (or $(c/\beta)^{1/2}$ in dimensional form corresponding to ~11° latitude) and $\lambda = R/5$, where $R = 6.3 \times 10^6$ m denotes the radius of the Earth. Other constants are assigned the following values: $c = 30$ m s^{-1}, $g = 9.8$ m s^{-2}, $\beta = 2.0 \times 10^{-11}$ m^{-1} s^{-1}, and $a = 2.5$. The value of c corresponds to the observed stratospheric Kelvin waves, which are believed to be forced from troposphere (Holton, 1973; Chang, 1976). This value also implies a phase speed of ~10 m s^{-1} for the gravest Rossby mode and slower phase speed for higher Rossby modes, in order-of-magnitude agreement with observed tropical Rossby-type waves.

The results presented below are computed up to zonal wavenumber 29 and Hermite mode 29 to ensure accuracy better than 99.9%.

a. Slow forcing: Rossby wave and Kelvin wave response

In this first case we set $\tau = 1$ day, which gives a relatively slow forcing. The variation of the forcing amplitude with time is shown in Fig. 3. Fig. 4 shows the velocity and geopotential for days 2, 3, 4, 6 and 9 after the forcing is turned on.

On day 2, a high-pressure center is building up over the area of forcing with a slightly subgeostrophic anticyclonic outflow around it. The wind speed is stronger on the equatorward part of the circulation due to the smaller Coriolis parameter. Southward of 15°N the wind becomes noticeably cross isobaric and flows across the equator, backing sharply from northeasterly to westerly in the process. Twenty-four hours later (day 3), the flow strengthens and becomes more geostrophic. The backing of the cross-equatorial flow becomes more pronounced resulting in a distinct eastnortheast–westsouthwest equatorial shear line located southeast of the high. On day 4, a vortex (area *a* in Fig. 4) develops on the equatorial shear line. South of the shear line a southwesterly cross-equatorial flow is established. Further east, a band of westerly wind distributed symmetrically about the equator (area *b*) shows up and appears to propagate eastward.

On day 6, the equatorial vortex drifts southwestward and begins to develop around it a small high pressure area just south of the equator. The mid-

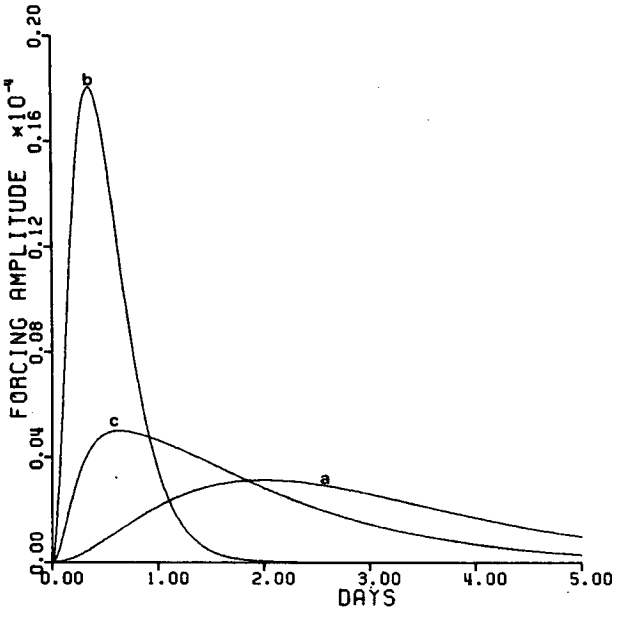

FIG. 3. Variation of forcing amplitude with time. Curve *a* is for the first case (slow forcing with $\tau = 1$ day), curve *b* for the second case (fast forcing with $\tau = 15 \times 10^3$ s) and curve *c* for the third case (multiple time scale "realistic" forcing). Curves *a*, *b* and *c* are normalized such that the areas under them are equal.

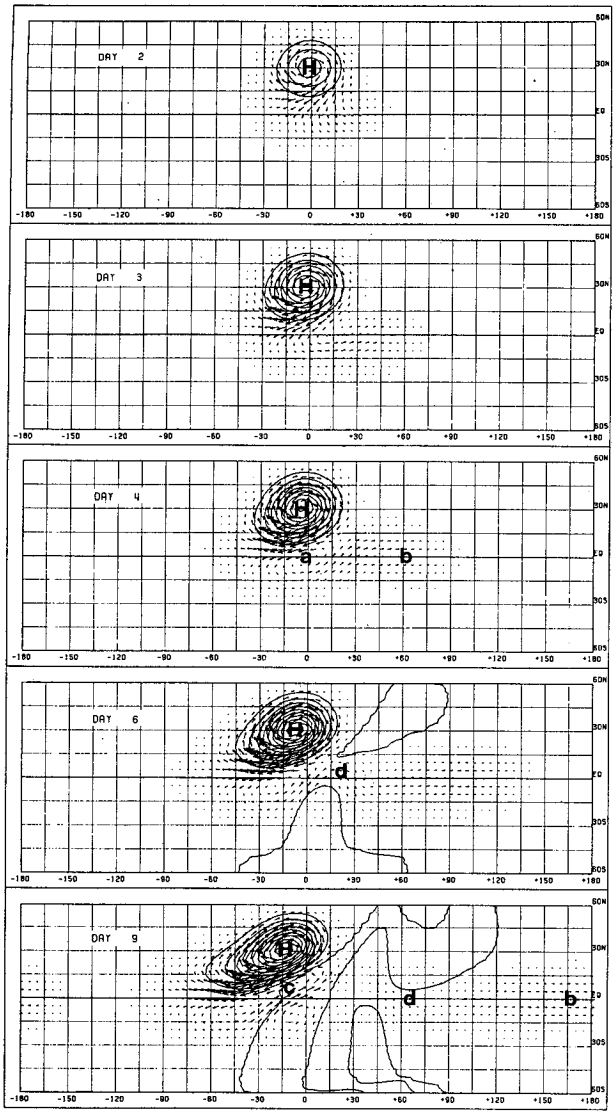

FIG. 4. The velocity and geopotential (solid lines) fields for days 2, 3, 4, 6 and 9 for the slow forcing case (τ = 1 day). See text for details.

latitude anticyclone now shows a marked northeast–southwest tilt with a ridge line extending toward the equator. Parallel to this ridge line a band of low pressure appears to the east. The southwesterly cross-equatorial flow strengthens and makes a distinct wave (area *d*) as it swings back south to merge with the eastward propagating equatorial westerlies.

By day 9, the northeast–southwest tilt of the midlatitude anticyclone becomes very pronounced. A streak of strong northeasterly winds surges from about 25°N to near the equator. Between this northeasterly streak and the southwesterly cross-equatorial flow, a very marked shear line is developed and extends from just south of the equator up to about 15°N (area *c*). This shear line also roughly divides a general area of high pressure to its west from a band of low pressure to its east. This large area of complex motions which constitutes the major response of the tropical atmosphere to the midlatitude forcing drifts slowly westward with the midlatitude anticyclone. The equatorial wave (area *d*) and westerlies (area *b*) propagate further to the east and become detached from this area of major response.

In order to ascertain the identity of the response, a mode-by-mode computation was carried out. Figs. 5a–5f show the velocity field of all wave modes of $n = -1$ and 0 and the Rossby modes of $n = 1$, 2, 3 and 4, respectively, while Fig. 5g shows the combined velocity field of the Rossby modes $n = 1$ to 9, all for day 9. Comparing Fig. 5 and Fig. 4, it is clear that the main response which drifts slowly westward is a congregation of Rossby waves, while the eastward propagating equatorial wave (*d*) and westerlies (*b*) are manifestations of the mixed Rossby–gravity and Kelvin waves, respectively. (Although mixed Rossby–gravity waves have westward phase speed, their group velocity is always eastward.) The computation also shows that for this slow, large-scale forcing, the inertia–gravity waves excited are negligible.

The development of the main response may be interpreted in terms of wave-group behavior of the Rossby waves of different Hermite modes. For each Hermite mode (*n*), Rossby waves of different zonal wavenumber combine to form a wave group with a zonal width comparable to the longitudinal extent of the forcing. Outside of the width of the wave group, disturbances due to that Hermite mode are of negligible amplitude. Within the width of the wave group, the disturbances resemble that of half a wavelength of a simple wave as shown in Figs. 4c and 5c of Matsuno (1966).

The wave groups of the lower Hermite modes, $n = 1$–3 have local wavenumber near three while those of higher modes, $n = 4$–7, have local wavenumber near five. All of these wave groups have westward group velocity but the speed is smaller for the higher modes. The wave group $n = 1$ therefore moves fastest to the west, followed successively by wave groups of increasing n. As time goes on, the wave groups of different n drift further and further apart. Now, since equatorial motions are mainly made up of contributions from lower modes while midlatitude motions are mainly made up of contributions from the higher modes, the development of a northeast–southwest tilt in the midlatitude anticyclone and the equatorial disturbances may be seen as a natural consequence of the gradual westward displacement of the lower mode wave groups relative to the higher mode wave groups. The strong northeasterly streak is built up with contributions

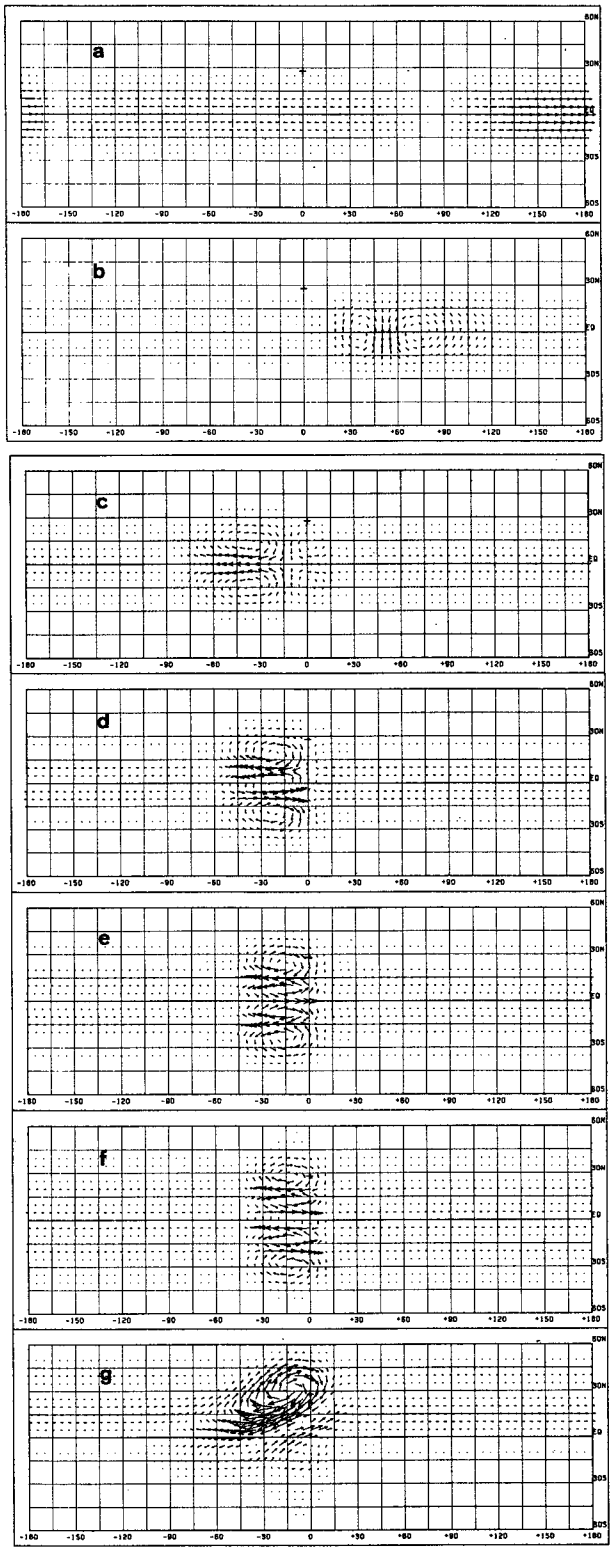

FIG. 5. The wave groups of different Hermite modes at day 9 after the slow forcing (τ = 1 day) is turned on: (a) Kelvin wave group ($n = -1$); (b) mixed Rossby–gravity wave group of $n = 0$; (c)–(f) Rossby wave groups of $n = 1$–4, respectively; (g) the combined velocity field of Rossby wave groups of $n = 1$–9. For the same speed, the vectors in (a) and (b) are drawn five times longer than those in (c)–(g).

from many Hermite modes; modes 1–2 make up the far southwest end of the streak while modes 4–5 make up the northeast part. The southwesterly cross-equatorial flow is made up mostly of contributions from modes 2–6. As the lower modes move further and further westward, their influences on the eastern part of the disturbance diminish and the motions there gradually develop higher mode characteristics.

b. Fast forcing: Mixed Rossby–gravity wave and inertia–gravity wave response

In our second case, we set $\tau = 15 \times 10^3$ s, or ~4 h. The variation of the forcing amplitude with time is shown in Fig. 3. It will be shown that the tropical response to this fast forcing has pronounced mixed Rossby–gravity wave and inertia–gravity wave components in addition to Rossby waves. The wind and geopotential fields are shown in Fig. 6. Because the flow fields change rapidly, all days from day 1–9 are shown.

On day 1, a belt of strong northerly and northeasterly wind sweeps across the equator. Near the leading edge, the wind blows perpendicular to the isobars away from the high pressure. This reveals strong gravity wave characteristics in the initial equatorward propagation of disturbances. More gravity wave characteristics are exhibited on day 2 when a low center and southerly winds appear behind the leading surge winds which have now penetrated deep into the Southern Hemisphere and deflected eastward. From day 3 onward to day 9, the process of separation of the Rossby modes and the gravity modes unfolds as in the first case. The Rossby modes drift slowly westward and, as in the case of the slow forcing, develop a markedly northeast–southwest oriented ridge pattern and, southeast of it, a sharp shear line (area *c*) between a strong northeasterly wind streak and a southwesterly cross-equatorial flow.

The eastward propagating disturbances are led by a Kelvin wave group which is easily identifiable by the band of westerlies distributed symmetrically about the equator. In addition, disturbances associated with large alternating cross-equatorial flows are observed to follow behind the Kelvin wave group, propagating eastward at about half the speed of the Kelvin modes. These disturbances have complex structures and change rapidly from day to day. On closer inspection, it may be detected that similar flow patterns appear to recur every three days. On days 4 and 7, a broad band of northerly cross-equatorial flow is observed (area *e*). Twenty-four hours later, this northerly band weakens and splits into

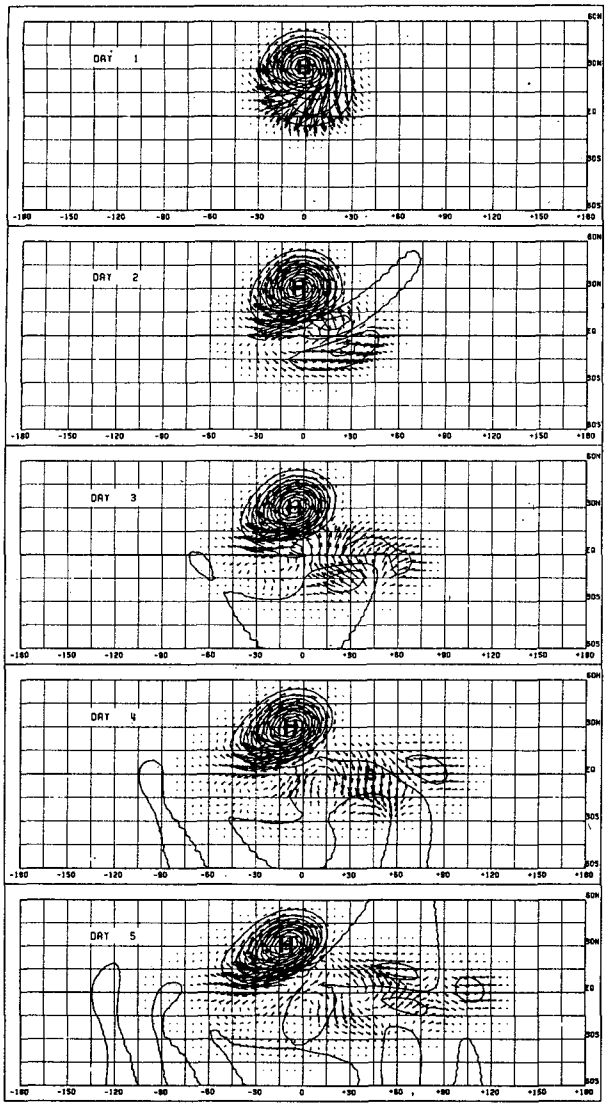

FIG. 6. The velocity and geopotential (solid line) fields for days 1–9 for the fast forcing case ($\tau = 15 \times 10^3$ s). See text for details.

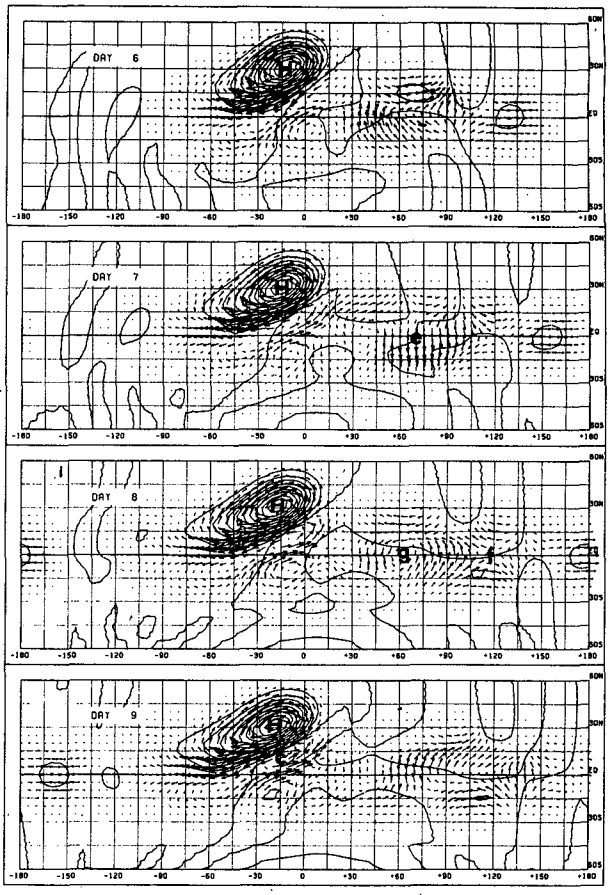

FIG. 6. (*Continued*)

two; one of them shifts slightly westward while the other moves far eastward. A band of southerly cross-equatorial flow develops in between, to the east and west of which a col (area f) and a vortex (area g) pattern appears. This southerly band spreads eastward and westward, weakening in the middle (days 6 and 9), and in another 24 h is replaced by northerlies.

The flow patterns of a col and a vortex around areas c and d, respectively, provide clues as to the identity of these disturbances. A comparison of these flow patterns with Figs. 6a, 6b and 7 of Matsuno (1966) clearly indicates that the disturbances are due to the two $n = 0$ Hermite modes—mixed Rossby–gravity and eastward propagating inertia–gravity waves. This identification is confirmed by Fig. 7 which shows the total $n = 0$ modes for days 4–9. The mixed Rossby–gravity and inertia–gravity quasi-periodic evolution of the flow pattern may be interpreted in terms of wave group behavior of these two modes. For each mode the waves of different zonal wavenumber combine to form a wave group of local wavenumber 5. From (6) the phase velocity c_p and the group velocity c_g of the wave groups for local wavenumber five are as follows:

Mixed Rossby–gravity waves	Inertia–gravity waves
$c_p = -19.3$ m s^{-1}	$c_p = 49.3$ m s^{-1}
$c_g = 8.5$ m s^{-1}	$c_g = 21.5$ m s^{-1}
$c_p - c_g = -27.8$ m s^{-1}	$c_p - c_g = 27.8$ m s^{-1}

Individual wavelets of the mixed Rossby–gravity wave ($M1$, $M2$, $M3$ and $M4$ in Fig. 7) move westward relative to the wave groups (line MM). They appear to be generated at the eastern edge of the wave group and grow in amplitude as they propagate toward the center of the wave group. After passing the center of the wave group, their amplitude diminishes and finally the wavelets disappear as they move

out of the wave group towards the west. The relative velocity of the wavelets with respect to the wave group is -27.8 m s^{-1} and this means that a complete wave of wavenumber 5 moves through the center of the wave group in 3.3 days. A similar description may be given for the inertia–gravity wave group except that now the wavelets ($G1$, $G2$, $G3$ and $G4$) move eastward relative to the wave group (line GG). Figure 7 clearly shows that a superposition of these two wave groups results in the complicated flow pattern which propagates eastward at 15 m s^{-1} (the average of the group velocities of the wave groups) and evolves quasi-periodically with a period of about three days.

c. *Response to a "realistic" midlatitude pressure surge*

In this case, we present an example of the response of the tropical atmosphere to a multiple time-scale pressure surge which rises rapidly to a maximum within ~12 h, and then falls off exponentially with an e-folding time ~1 day (Fig. 3). This forcing is constructed with a linear combination of three forcings of the form (3) with $\tau_1 = 15\,000$ s, $\tau_2 = 35\,000$ s, $\tau_3 = 70\,000$ s and weights 0.6 τ_1, 0.7 τ_2 and 0.55 τ_3, respectively. The solution for this combined forcing is then given by a linear combination of the solutions for each of the component forcing with the same weights.

Fig. 8 shows the flow pattern at days 2 and 7. The response at day 2 resembles a typical early monsoon surge flow with well developed quasi-geostrophic northeasterly wind sweeping down from about 25°N to near the equator. Gravity-wave characteristics are evident only in the southern equatorial region where the cross-equatorial flow backs sharply and begins to spread the disturbances eastward. By day 7, the process of separation of the different modes of motion is well advanced. The Rossby modes form a tilting high pressure ridge with a strong northeasterly wind streak to its south. At the longitudes of the forcing, a southwesterly cross-equatorial flow has developed, forming between it and the northeasterly wind streak a strong equatorial shear line (area c). All these patterns are essentially the same as those in the first case. The effects of the midlatitude pressure surge are spread eastward along the equator by the Kelvin (area b), mixed Rossby–gravity and $n = 0$ inertia–gravity modes. Compared to the second case, the amplitudes of the $n = 0$ modes are much smaller with the mixed Rossby–gravity mode dominating over the inertia–gravity mode.

Finally, it may be worth noting that although the wind speed associated with the mixed Rossby–gravity mode and the inertia–gravity mode is about one order of magnitude smaller than that associated with the Rossby modes, the divergence fields (not shown) produced by them are of comparable magnitudes.

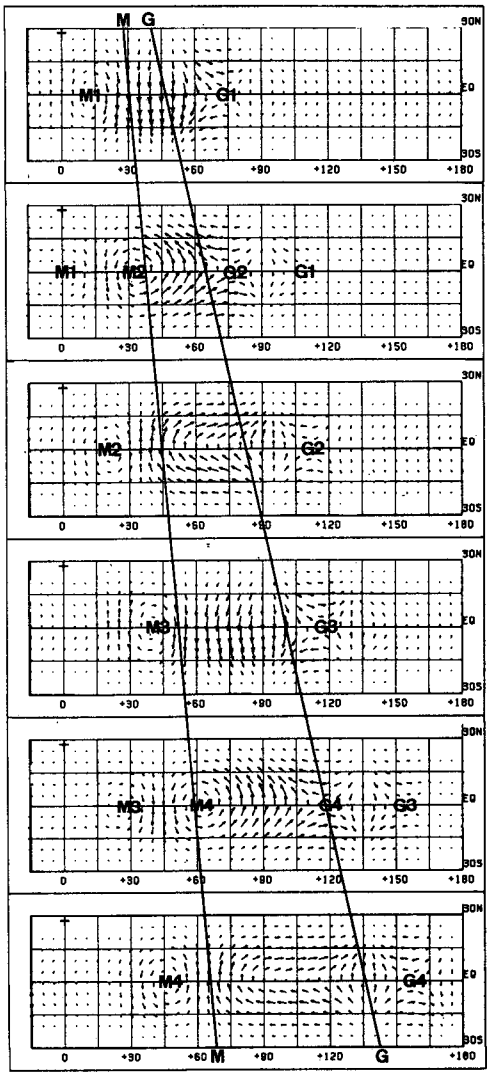

FIG. 7. $n = 0$ Hermite modes excited by the fast forcing from day 4 (top) to day 9 (bottom). Thick line MM marks the trajectories of the center (area of maximum amplitude) of the mixed Rossby–gravity wave group; and GG that of the inertia–gravity wave group. Individual wavelets move through the wave groups as shown by the movement of the center of wave patterns $M1$, $M2$, $M3$, $M4$ and $G1$, $G2$, $G3$, $G4$.

4. Discussion

The simple model presented here shows that the theoretical tropical response to midlatitude surge forcing consists of three main components: Rossby modes, $n = 0$ (mixed Rossby–gravity and inertia–gravity) modes, and the Kelvin mode. All $n > 0$ inertia–gravity modes are negligible for forcing comparable to normal monsoon surge conditions. In this

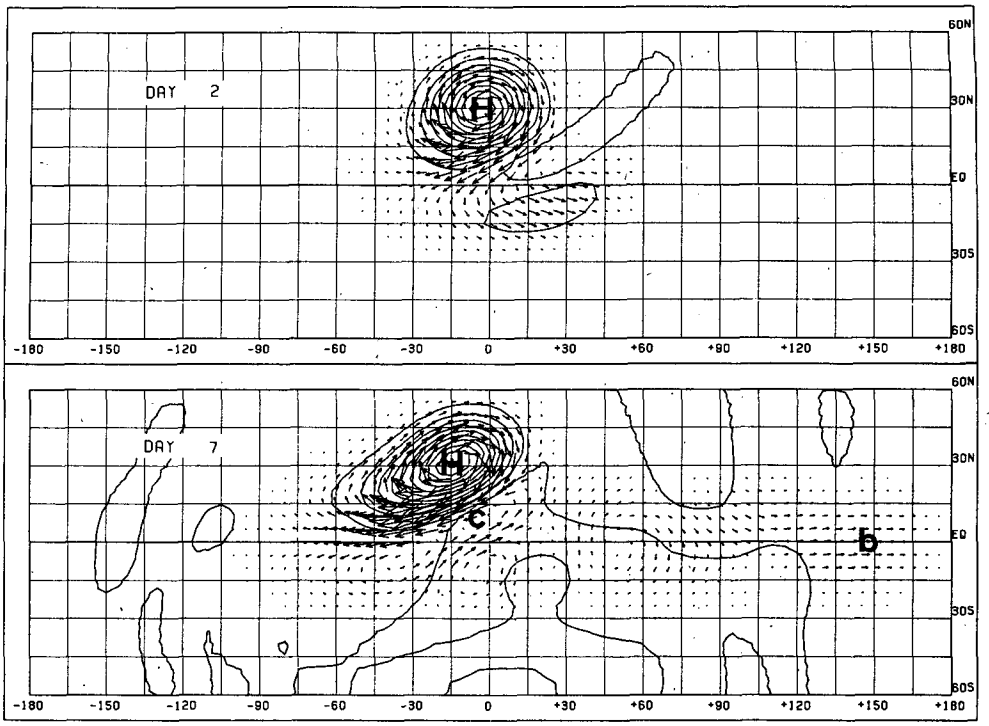

FIG. 8. The velocity and geopotential fields for days 2 and 7 for the multiple time scale "realistic" forcing. See text for details.

section we shall attempt to compare these theoretical solutions with previous observational and theoretical studies.

The disturbances of Rossby-wave origin propagate slowly to the west but remain for all relevant time near to the longitudes of forcing. The motion is quasi-geostrophic with large geopotential perturbations and strong winds. They account for a large proportion of the kinetic energy and potential energy of the forced motion.

In this Rossby mode of response, we find many features that are reminiscent of typical flow patterns during a winter monsoon season. Our solutions indicate that following a pressure surge in the midlatitudes, a belt of strong winds rapidly builds up, sweeping down from about 20°N to the equator and veering gradually from northnortheasterly to eastnortheasterly. This wind belt appears to correspond to the wind surges observed over the South China Sea which often develop within 24 h after a steep pressure rise occurs in southern China. Although the flow pattern is basically a feature of the Rossby type motion, its development however, is not through the usual mechanism of vorticity advection but through a process of separation of the Rossby-mode response from the gravity-mode responses. In a way, we may regard this process as a "geostrophic" adjustment process on a β plane. The velocity scale therefore is the gravity wave speed and not the advective speed. This may account for the rapid propagation of the wind surge over the South China Sea as noted by Ramage (1971) and Chang *et al.* (1979).

The northeasterly wind belt predicted by the theory, however, is too broad and penetrates further westward than observed. More realistic predictions could possibly be made had the effects of surface friction and orography been considered. Since wind surges over the South China Sea occur mainly in the lowest one kilometer of the atmosphere, frictional dissipation could significantly reduce the wind speed over land and thereby leave a narrower wind belt over the ocean. The westward extent of the surge also would be curtailed by the mountain ranges of Indochina and the Malayan Peninsula as the barrier effect would be significant for the shallow layer of strong winds.

Due to the very unbalanced state, the initial response to the pressure surge is mainly of gravity-type motions. The solution in this regard resembles the strong northerly wind observed immediately after the onset of a surge. As time progresses the Rossby modes are gradually established resulting in a larger easterly component in the equatorward jet streak. This shift of wind direction is qualitatively in agreement with composite studies carried out at the Singapore Meteorological Service (Chiyu, 1979).[3]

[3] Chiyu, T., 1979: Private communication.

An interesting finding of our study is the development, simultaneously with that of the surge wind belt, of a southwesterly cross-equatorial flow to the southeast of the surge belt. The resultant flow pattern—two opposing streams sandwiching an east-northeast–westsouthwest oriented equatorial shearline—resembles the typical winter synoptic situation depicted in Fig. 1. The cyclonic circulation (area *c* in Figs. 4, 6 and 8) developed on day 7 of all cases is in good agreement with the quasi-stationary cyclonic vortex observed near the northwest coast of Borneo during winter (Chang *et al.*, 1979; Houze *et al.*, 1981; Johnson and Priegnitz, 1981). Bryant's (1958) Fig. 2 shows that this northern equatorial cyclonic circulation is sometimes accompanied by a high to its southwest and a low to its southsoutheast. This setup also is present in all our results. The basic mechanism of the establishment of this flow pattern has so far not been elucidated. An inspection of the local orography may suggest that the southwesterly flow has simply resulted from a deflection of the northeasterly winds by the mountain barriers along the southern coast of the South China Sea. The quasi-stationarity of this flow pattern lends support to this conjecture since it would appear that the flow pattern is somehow locked onto the orographic features. However, our results allow us to propose instead that such a pattern is a basic feature of the Rossby-mode response of the tropical atmosphere to a large-scale pressure forcing in the midlatitudes.

The development of this cyclonic circulation and shear pattern depends on the establishment of the strong northeasterly wind belt to the southeast of the main high pressure center, and a cross-equatorial southwesterly flow further to the east. As discussed in Section 3a, the strong northeasterly wind belt with a northeast–southwest orientation is due to the combination of two facts: 1) the differential westward movement of the Rossby modes with a faster group velocity for the lower modes, and 2) the smaller Coriolis parameter on the equatorial side of the high center. The establishment of the southwesterly cross-equatorial flow may be seen from the distribution of the individual modes shown in Fig. 5. Only *n*-even modes have nonzero meridional velocity at the equator, and southeast of the main anticyclone it is southerly for $n = 2, 6, \ldots$ and northerly for $n = 4, 8, \ldots$ for all days considered. Since the expansion coefficient p_n of the forcing specified by (11) decreases steadily from $n = 2$ toward higher n for all reasonable ranges of a (central latitude) and σ (meridional scale) of the forcing function, the amplitude of $n = 2$ is greater than that of $n = 6$, and the amplitude of $n = 4$ is greater than that of $n = 8$, etc. Thus the total cross-equatorial flow is southerly. For the zonal wind component in this area, it can be seen that $n = 1, 3$ both give westerlies at the equator, resulting in a cross-equatorial southwesterly flow. This flow remains through all relevant time because of the slow speed for all Rossby modes and the relatively large zonal wavelength for the lower modes. Thus the cyclonic flow southeast of the forcing region is a consequence of the Rossby wave group whenever a surge forcing occurs. Its development is an inherent feature of the equatorial β-plane dynamics and does not need the presence of orography. The latter, however, appears certain to play at least a modificatory role in the real atmosphere over the South China Sea.

The possibility of remote forcing of equatorial motions through mixed Rossby–gravity, inertia–gravity and Kelvin mode responses is another interesting implication of our results. Interpretation of equatorial flow fields in terms of Kelvin-wave response to local forcing has been suggested by Webster (1972, 1973) and Chang (1976). However some investigators in the past (Mak, 1969; Wallace, 1973) have not discussed the possibility of Kelvin waves being forced from midlatitudes, because the absence of a meridional wind component means there is no meridional pressure flux associated with these waves. Our results suggest that significant Kelvin wave disturbances may be excited by midlatitude forcing. In this case the initial forcing excites gravity type motions represented by the transient part of the solutions. As the air surges to the equatorial region it is deflected and propagates westward or eastward as wave groups in the adjustment process. The westward groups become organized mainly into Rossby modes and the eastward groups into mixed Rossby–gravity, inertia–gravity ($n = 0$) and Kelvin modes. Hence it appears that whenever an unbalanced initial state is present, Kelvin waves may be excited by midlatitude forcing.

The forced Kelvin wave solution has another interesting aspect. The zonal velocity and height perturbation of the forced Kelvin wave are given by the first term of Eqs. (B3) and (B5) of Appendix B

$$u = \frac{g\Phi_0 D_0(\zeta)\exp[ik(ct - x)]}{2c(1 + ikc\tau)^3},$$

$$h = \frac{\Phi_0 D_0(\zeta)\exp[ik(ct - x)]}{2(1 + ikc\tau)^3}.$$

For a given forcing component $\phi_0 D_0(\zeta)$ and a time scale τ, it is evident that both u and h increase with decreasing k. Thus for a white noise forcing the largest response is in the lowest wavenumber. This result is similar to the baroclinic Kelvin waves forced by heating as shown by Webster (1973) for a two-level steady case and by Chang (1976) for the general case. Our result also shows that for a slower forcing time scale (large τ) the total Kelvin mode response will be smaller but the distribution of energy will be more biased favoring larger zonal wavelength. On the other hand, a faster forcing time

scale (small τ) leads to large total Kelvin mode response with a more uniform distribution among all wavenumbers. Even though the solutions given here are for specific forcing functions, these behavior patterns will remain qualitatively valid for all reasonable time variations of the forcing function.

At the present, observational evidence for the eastward propagating equatorial motion is somewhat scanty. The well-known findings reported are the stratospheric Kelvin waves presumably forced from tropospheric sources (Wallace, 1973) and the 40–50 day tropospheric oscillations observed by Madden and Julian (1971, 1972). Recently, Lyons (1981) found a wavenumber-one spectral peak in the 200 mb vorticity that resembles a Kelvin wave; however, he associated it with forcings from tropical heat sources. The evidence most relevant to our results was reported by Williams (1981) in a study of the Winter MONEX data. His observation of a slow rise of pressure over western Indonesia and the acceleration of westerly flows a few days after a cold surge crosses the South China coast seems to correspond to the equatorial features of our Rossby-mode response (Fig. 8, day 7). Further to the east, his observation of an eastward propagating westerly flow with embedded cloud clusters may be identified with the mixed Rossby–gravity, inertia–gravity and Kelvin wave groups.

Our result shows that several observed tropical developments following the winter monsoon surges are represented by the theoretical responses of days 6–7. Since a pressure pattern resembling actual surge onset conditions is not established until days 2–3 in the model, the tropical response time corresponds to four days after the surge onset. This time is comparable, although somewhat slower, than the observed 1–4 days response time (Chang *et al.*, 1979; Chang and Lau, 1980, 1981). In fact, the choice of c, which gives the limit of group velocity for any wave motion in the system and is related to the equivalent depth of the motion, influences significantly the speed of development. Our choice of $c = 30$ m s^{-1} is based on an estimate of the observed stratospheric Kelvin waves which are believed to be induced by tropospheric random forcing (Holton, 1973; Chang, 1976). However, the cold surges could have their own equivalent depths that may make the development in the model faster.

The day 9 solutions are shown principally for the prupose of allowing the different Hermite modes to separate out more completely, therefore making it easier to identify the various modes. On the other hand, since cold air surges occur repeatedly during winter, it is reasonable to expect day 9 to represent a "time-mean" condition during the northeast monsoon. In this regard the observed seasonal mean northeast wind belt extending from the vicinity of Taiwan to the southern South China Sea, and the mean equatorial trough from Borneo to Philippines, are quite well simulated.

5. Concluding remarks

Using a simple shallow-water equation model, we have shown that many features of the tropical motion over the South China Sea during the northeast monsoon may be interpreted as linear wave responses to midlatitude forcings. Our main findings are as follows:

1) Midlatitude forcing with large time and space scales excite mainly Rossby and, to a much smaller amplitude, Kelvin waves. As either of these scales decreases, the amplitudes of mixed Rossby–gravity and inertia–gravity waves increase.

2) Immediately following a pressure forcing, the strong wind surge is more northerly with a gravity wave character. The strong cross-isobaric divergent flow occurs without the presence of surface friction. It becomes more easterly as the Rossby wave group is established, in agreement with observations.

3) The development of the main tropical flow pattern after a midlatitude pressure forcing, including the strong northeast wind belt southeast of the main anticyclone and a cyclonic shear zone further southeast of it, is represented by the slowly moving Rossby wave group response.

4) This Rossby wave group develops a pronounced northeast–southwest tilt which is caused by the differential westward movement of wave modes, with the lower modes having relatively faster group velocities.

5) The equatorial cyclonic shear flow southeast of the main anticyclone is an inherent property of the Rossby wave group response even in the absence of orography. It is consistent with the mean winter condition of a northeast–southwest equatorial trough along Borneo–Philippines, and with an enhanced cyclonic circulation over Borneo following surges.

6) The surge forcing also gives rise to eastward moving wave groups of the Kelvin, mixed Rossby–gravity, and inertia–gravity (mainly $n = 0$) modes. This result suggests a possible interpretation for the eastward moving cloud patterns observed recently during winter.

7) The Kelvin waves forced by midlatitude forcing, as is the case for the thermally forced Kelvin waves, have more energy in the larger wavelengths for a white noise random forcing.

It appears that the diverse events of the monsoon surge might be given a coherent interpretation in terms of simple, inviscid, barotropic β-plane dynamics. However, many important questions remain. Our theory cannot furnish any information on the vertical structure of monsoon surges and

responses, and is not easily extended for consideration of many other important physical effects such as variable zonal mean wind or orography. Further studies in the following three directions should therefore be carried out. First, numerical barotropic models may throw some light on the effects of spherical geometry, nonlinearity, orography and variable mean zonal winds on monsoon surges. Second, analytical and numerical studies of the corresponding baroclinic problems will give a better understanding of the vertical structure of surges. And last, but not least, more detailed observational studies are needed to check the predictions of such dynamical theories.

Acknowledgments. We wish to thank Drs. K. M. Lau and R. T. Williams for helpful discussions. One of us (HL) wishes to thank the Director, Meteorological Service Singapore, for granting a 1-year study leave to do research at the Naval Postgraduate School. This work was supported by the National Science Foundation, Division of Atmospheric Sciences, Global Atmospheric Research Program, under Grant ATM 80-13153.

APPENDIX A

List of Symbols

a latitude of the center of forcing in units of $(c/\beta)^{1/2}$

c phase speed of free gravity wave $[=(gH)^{1/2}]$

c_g group velocity

c_p phase velocity

$D_n(\zeta)$ Hermite function of order n. $D_n(\zeta)$ is the bounded solution of the equation

$$\frac{d^2D_n(\zeta)}{d\zeta^2} + (2n + 1 - \zeta^2)D_n(\zeta) = 0$$

and is normally written as $H_n(\zeta) \times e^{-\zeta^2/2}$, where $H_n(\zeta)$ is the Hermite polynomial of order n:

$$H_n(\zeta) = (-1)^n e^{\zeta^2} \frac{d^n}{d\zeta^n} e^{-\zeta^2}$$

g gravitational acceleration (=9.8 m s^{-2})

h^T, u^T, v^T, ϕ^T time-Fourier transform of the x-Fourier coefficients of h', u', v' and ϕ', respectively (see ξ^T)

h' perturbation of fluid depth from H

H constant depth of the unperturbed fluid

k $k = (2\pi m)/L$

L circumference of the Earth at the equator $(=2\pi R)$

m number of waves in x

p_n expansion coefficient of the ζ-profile of the forcing function in terms of $D_n(\zeta)$:

$$\exp\left[-\frac{1}{2}\left(\frac{\zeta - a}{\sigma}\right)^2\right] = \sum_{n=0}^{\infty} p_n D_n(\zeta)$$

R radius of the Earth $(=6.3 \times 10^7$ m)

t time

u' eastward velocity component

x eastward coordinate

y northward coordinate

β rate of change of the Coriolis parameter in y-direction; $\beta = 2 \times 10^{-11}$ (m s)$^{-1}$

γ_n $\gamma_n = 1 + \omega_n^2\tau^2$

ζ nondimensionalized y coordinate; $\zeta = (\beta/c)^{1/2}y$

λ half width of the x profile of the forcing function

ξ_n expansion coefficient of ξ^T in terms of the Hermite functions

$$\xi^T = \sum_{n=0}^{\infty} \xi_n D_n(\zeta)$$

ξ^T time-Fourier transform of the x-Fourier coefficients of the variable ξ'

$$\left[= \int_{-\infty}^{+\infty} (\xi_c' + i\xi_s')e^{-i\omega t}dt\right]$$

ξ' dummy variable to represent u', v', h' or Φ'

ξ_c', ξ_s' coefficients of expansion of the variable ξ' in a Fourier series in x direction:

$$\xi' = \sum_{m=0}^{\infty} \left[\xi_c'(m, y, t) \cos\frac{2\pi m}{L}x + \xi_s'(m, y, t) \sin\frac{2\pi m}{L}x\right]$$

σ nondimensionalized half-width of the ζ-profile of the forcing function

τ time constant of the forcing function

Φ_n expansion coefficient of Φ^* in terms of the Hermite functions;

$$\Phi^* = \sum_{n=0}^{\infty} \Phi_n D_n(\zeta)$$

Φ_c, Φ_s expansion coefficient of the space-dependent part of the forcing function in a Fourier series in x direction

Φ' forcing function

Φ^* $\Phi^* = \Phi_c + i\Phi_s$

ω	angular frequency of waves; parameter of time-Fourier transforms.
ω_n	$\omega_n = [(2n + 1)\beta c]^{1/2}$
$\omega_{n0}, \omega_{n1}, \omega_{n2}$	angular frequencies of the Hermite-mode-n Rossby wave, westward and eastward propagating inertia–gravity waves, respectively. When $n = 0$, ω_{00} denotes the angular frequency of the mixed mode and ω_{02} that of the eastward propagating inertia-gravity wave

APPENDIX B

Solutions of Equations

The solutions of Equations with forcing specified in Eq. (3) are as follows:

$$\left.\begin{aligned}
u'(x,\zeta,t) &= \sum_{n=0} -g\beta[(n+1)\Phi_{n+1} - \tfrac{1}{2}\Phi_{n-1}](nD_{n-1} + \tfrac{1}{2}D_{n+1})[U_n(t) + \omega_n^{-2}] + \sum_{m=1}^{\infty} u\left(\frac{2\pi m}{L}, \zeta, t\right), \\
v'(x,\zeta,t) &= \sum_{n=0}^{\infty} -g(\beta/c)^{1/2}[(n+1)\Phi_{n+1} - \tfrac{1}{2}\Phi_{n-1}]D_n V_n(t) + \sum_{m=1}^{\infty} v\left(\frac{2\pi m}{L}, \zeta, t\right), \\
h'(x,\zeta,t) &= \Phi'(x,\zeta,t)\{1 - e^{-t/\tau}[t^2/(2\tau^2) + t/\tau + 1]\} \\
&\quad + \sum_{n=0}^{\infty} \beta c[(n+1)\Phi_{n+1} - \tfrac{1}{2}\Phi_{n-1}](nD_{n-1} - \tfrac{1}{2}D_{n+1})[U_n(t) + \omega_n^{-2}] + \sum_{m=1}^{\infty} h\left(\frac{2\pi m}{L}, \zeta, t\right),
\end{aligned}\right\} \quad \text{(B1)}$$

where

$$\left.\begin{aligned}
U_n(t) &= [(\gamma_n - 1)^{1/2}(\gamma_n - 4)\sin\omega_n t - (4 - 3\gamma_n)\cos\omega_n t]/(\omega_n^2\gamma_n^3) \\
&\quad - \frac{1}{2\gamma_n}[t^2 + 2\tau(\gamma_n + 2)t/\gamma_n + 2\tau^2(\gamma_n^2 + \gamma_n + 4)/\gamma_n^2]e^{-t/\tau}, \\
V_n(t) &= [(4 - 3\gamma_n)\sin\omega_n t + (\gamma_n - 1)^{1/2}(\gamma_n - 4)\cos\omega_n t]/(\omega_n\gamma_n^3) \\
&\quad + \frac{1}{2\tau\gamma_n}[t^2 + (4t\tau/\gamma_n) - (2\tau^2/\gamma_n) + (8\tau^2/\gamma_n^2]e^{-t/\tau},
\end{aligned}\right\} \quad \text{(B2)}$$

$$\begin{aligned}
u(k,\zeta,t) &= \frac{g\Phi_0 D_0 e^{ik(ct-x)}}{2c(1 + ikc\tau)^3} + \frac{g\beta}{2}\Phi_1 D_1[P_1(\omega_{00};\omega_{02},kc)e^{i(\omega_{00}t-kx)} + P_1(\omega_{02};\omega_{00},kc)e^{i(\omega_{02}t-kx)}] \\
&\quad + \sum_{n=1}^{\infty}\sum_{p=0}^{2} g\beta\Big\{[n(n+1)\Phi_{n+1}D_{n-1} - \tfrac{1}{4}\Phi_{n-1}D_{n+1}]P_1(\omega_{np};\omega_{nq},\omega_{nr}) + \frac{n+1}{2}\Phi_{n+1}D_{n+1}(\omega_{np} + kc) \\
&\quad \times P_1(\omega_{np};\omega_{nq},\omega_{nr},kc) - \frac{n}{2}\Phi_{n-1}D_{n-1}(\omega_{np} - kc)P_1(\omega_{np};\omega_{nq},\omega_{nr},-kc)\Big\}e^{i(\omega_{np}t-kx)} \\
&\quad + \frac{ig\tau k\Phi_0 D_0}{2}P_2(kc,-kc)Q(kc,-kc)e^{-[ikx+(t/\tau)]} + \frac{g\tau^2\beta\Phi_1 D_1}{4}P_2(\omega_{02},\omega_{00},kc)Q(\omega_{02},\omega_{00},kc)e^{-[ikx+(t/\tau)]} \\
&\quad + \sum_{n=1}^{\infty}\Big\{\frac{ig\tau k\Phi_n D_n}{2}P_2(kc,-kc)Q(kc,-kc) + \frac{g\tau^2\beta[n(n+1)\Phi_{n+1}D_{n-1} - \tfrac{1}{4}\Phi_{n-1}D_{n+1}]}{2}P_2(\omega_{n0},\omega_{n1},\omega_{n2}) \\
&\quad \times Q(\omega_{n0},\omega_{n1},\omega_{n2}) + \frac{g\tau^2\beta(n+1)\Phi_{n+1}D_{n+1}}{4}P_2(\omega_{n0},\omega_{n1},\omega_{n2},kc_0)[(1 - ikc\tau)Q(\omega_{n0},\omega_{n1},\omega_{n2},kc) \\
&\quad - Q'(\omega_{n0},\omega_{n1},\omega_{n2},kc)] + \frac{g\tau^2\beta n\Phi_{n-1}D_{n-1}}{4}P_2(\omega_{n0},\omega_{n1},\omega_{n2},-kc) \\
&\quad \times [-(1 + ikc\tau)Q(\omega_{n0},\omega_{n1},\omega_{n2},-kc) + Q'(\omega_{n0},\omega_{n1},\omega_{n2},-kc)]\Big\}e^{-[ikx+(t/\tau)]},
\end{aligned} \quad \text{(B3)}$$

$$v(k,\zeta,t) = ig(\beta/c)^{1/2}D_0\Phi_1[P_1(\omega_{00};\omega_{02})e^{i(\omega_{00}t-kx)} + P_1(\omega_{02};\omega_{00})e^{i(\omega_{02}t-kx)}] + \sum_{n=1}^{\infty}\sum_{p=0}^{2} ig(\beta/c)^{1/2}D_n$$
$$\times [(n+1)(\omega_{np}+kc)\Phi_{n+1} - \tfrac{1}{2}(\omega_{np}-kc)\Phi_{n-1}]P_1(\omega_{np};\omega_{nq},\omega_{nr})e^{i(\omega_{np}t-kx)}$$
$$- \frac{g\tau}{2}(\beta/c)^{1/2}D_0\Phi_1P_2(\omega_{02},\omega_{00})Q(\omega_{02},\omega_{00})e^{-[ikx+(t/\tau)]} - \sum_{n=1}^{\infty}\frac{g\tau}{2}(\beta/c)^{1/2}D_nP_2(\omega_{n0},\omega_{n1},\omega_{n2})e^{-[ikx+(t/\tau}$$
$$\times \{[(n+1)(1-ikc\tau)\Phi_{n+1} - \tfrac{1}{2}(1+ikc\tau)\Phi_{n-1}]Q(\omega_{n0},\omega_{n1},\omega_{n2})$$
$$- [(n+1)\Phi_{n+1} - \tfrac{1}{2}\Phi_{n-1}]Q'(\omega_{n0},\omega_{n1},\omega_{n2})\}, \quad \text{(B4)}$$

$$h(k,\zeta,t)$$
$$= \frac{\Phi_0D_0e^{ik(ct-x)}}{2(1+ikc\tau)^3} + \frac{\beta c}{2}\Phi_1D_1[P_1(\omega_{00};\omega_{02},kc)e^{i(\omega_{00}t-kx)} + P_1(\omega_{02};\omega_{00},kc)e^{i(\omega_{02}t-kx)}]$$
$$+ \sum_{n=1}^{\infty}\sum_{p=0}^{2}\beta c\left\{-[n(n+1)\Phi_{n+1}D_{n-1} + \tfrac{1}{4}\Phi_{n-1}D_{n+1}]P_1(\omega_{np};\omega_{nq},\omega_{nr}) + \frac{n+1}{2}\Phi_{n+1}D_{n+1}(\omega_{np}+kc)\right.$$
$$\left.\times P_1(\omega_{np};\omega_{nq},\omega_{nr},kc) + \frac{n}{2}\Phi_{n-1}D_{n-1}(\omega_{np}-kc)P_1(\omega_{np};\omega_{nq},\omega_{nr},-kc)\right\}e^{i(\omega_{np}t-kx)}$$
$$+ \frac{\Phi_0D_0}{2}P_2(kc,-kc)[-Q(kc,-kc) + Q'(kc,-kc)]e^{-[ikx+(t/\tau)]}$$
$$+ \frac{\beta c\tau^2\Phi_1D_1}{4}P_2(\omega_{02},\omega_{00},kc)Q(\omega_{02},\omega_{00},kc)e^{-[ikx+(t/\tau)]} + \sum_{n=1}^{\infty}\left\{\frac{\Phi_nD_n}{2}P_2(kc,-kc)\right.$$
$$\times [-Q(kc,-kc) + Q'(kc,-kc)] - \frac{\beta c\tau^2[n(n+1)\Phi_{n+1}D_{n-1} + \tfrac{1}{4}\phi_{n-1}D_{n+1}]}{2}P_2(\omega_{n0},\omega_{n1},\omega_{n2})$$
$$\times Q(\omega_{n0},\omega_{n1},\omega_{n2}) - \frac{\beta c\tau^2(n+1)\Phi_{n+1}D_{n+1}}{4}P_2(\omega_{n0},\omega_{n1},\omega_{n2},kc)[-(1-ikc\tau)Q(\omega_{n0},\omega_{n1},\omega_{n2},kc)$$
$$+ Q'(\omega_{n0},\omega_{n1},\omega_{n2},kc)] - \frac{\beta c\tau^2n\Phi_{n-1}D_{n-1}}{4}P_2(\omega_{n0},\omega_{n1},\omega_{n2},-kc)$$
$$\left.\times [-(1+ikc\tau)Q(\omega_{n0},\omega_{n1},\omega_{n2},-kc) + Q'(\omega_{n0},\omega_{n1},\omega_{n2},-kc)]\right\}e^{-[ikx+(t/\tau)]}, \quad \text{(B5)}$$

$$P_1(\omega_1;\omega_2,\omega_3,\ldots,\omega_n) = \frac{1}{(1+i\omega_1\tau)^3} + \prod_{j=2}^{n}\frac{1}{(\omega_1-\omega_j)},$$
$$P_2(\omega_1,\omega_2,\omega_3,\ldots,\omega_n) = \prod_{j=1}^{n}\frac{1}{(1+i\omega_j\tau)},$$
$$Q(\omega_1,\omega_2,\omega_3,\ldots,\omega_n) = (t/\tau)^2 + 2(t/\tau)S_1(\omega_1,\omega_2,\omega_3,\ldots,\omega_n) + 2S_2(\omega_1,\omega_2,\omega_3,\ldots,\omega_n),$$
$$Q'(\omega_1,\omega_2,\omega_3,\ldots,\omega_n) = 2[(t/\tau) + S_1(\omega_1,\omega_2,\omega_3,\ldots,\omega_n)], \quad \text{(B6)}$$
$$S_1(\omega_1,\omega_2,\omega_3,\ldots,\omega_n) = \sum_{j=1}^{n}\frac{1}{(1+i\omega_j\tau)},$$
$$S_2(\omega_1,\omega_2,\omega_3,\ldots,\omega_n) = \sum_{j=1}^{n}\sum_{k=j}^{n}\frac{1}{(1+i\omega_j\tau)(1+i\omega_k\tau)},$$

with

$$\Phi_{-1} = D_{-1}(\zeta) = 0,$$
$$\omega_n = [(2n+1)\beta c]^{1/2},$$

and

$$\gamma_n = 1 + \tau^2\omega_n^2.$$

REFERENCES

Bryant, K., 1958: Comparison of months giving extremes of rainfall during northeast monsoon at Changi, Singapore Island. *Meteor. Mag.*, **87**, 307–312.

Chang, C.-P., 1976: Forcing of stratospheric Kelvin waves by tropospheric heat sources. *J. Atmos. Sci.*, **33**, 740–744.

——, 1977: Viscous internal gravity waves and low-frequency oscillations in the tropics. *J. Atmos. Sci.*, **34**, 901–912.

——, J. E. Erickson and K. M. Lau, 1979: Northeasterly cold surges and near-equatorial disturbances over the Winter MONEX area during December 1974. Part I: Synoptic Aspects. *Mon. Wea. Rev.*, **107**, 812–829.

——, and K. M. Lau, 1980: Northeasterly cold surges and near-equatorial disturbances over the Winter MONEX area during December 1974. Part II: Planetary-scale aspects. *Mon. Wea. Rev.*, **108**, 298–312.

——, and ——, 1981: Planetary-scale motions of winter monsoons during cold surge and break periods. *Proc. Int. Conf. on Early Results of FGGE and Large-Scale Aspects of Its Monsoon Experiments*, Tallahassee, WMO, **4**, 12–19.

Holton, J. R., 1973: On the frequency distributions of atmospheric Kelvin waves. *J. Atmos. Sci.*, **30**, 499–501.

Houze, R. A., S. G. Geotis, F. D. Marks and A. K. West, 1981: Winter monsoon convection in the vicinity of North Borneo. Part I: Structure and time variation of the clouds and precipitation. *Mon. Wea. Rev.*, **109**, 1599–1618.

Johnson, R. H., and D. L. Priegnitz, 1981: Winter monsoon convection in the vicinity of North Borneo. Part II: Effects on large-scale fields. *Mon. Wea. Rev.*, **109**, 1619–1632.

Lighthill, M. J., 1965: Group Velocity. *J. Inst. Math. Applics.*, **1**, 1–28.

Lyons, S. W., 1981: Planetary-scale aspects of outgoing long-wave radiation and vorticity over the global tropics during winter. *Mon. Wea. Rev.*, **109**, 1773–1787.

Madden, R. A., and P. R. Julian, 1971: Detection of a 40–50 day oscillation in the zonal wind in the tropical Pacific. *J. Atmos. Sci.*, **28**, 702–708.

——, and ——, 1972: Description of global-scale circulation cells in the tropics with a 40–50 day period. *J. Atmos. Sci.*, **29**, 1109–1123.

Mak, M.-K., 1969: Laterally driven stochastic motions in the tropics. *J. Atmos. Sci.*, **26**, 41–64.

Matsuno, T., 1966: Quasi-geostrophic motions in the equatorial area. *J. Meteor. Soc. Japan*, **44**, 25–41.

Ramage, C. S., 1971: *Monsoon Meteorology*, Academic Press, 296 pp.

Wallace, J. M., 1973: General circulation of the tropical lower troposphere. *Rev. Geophys. Space Phys.*, **11**, 191–222.

Webster, P. J., 1972: Response of the tropical atmosphere to local steady forcing. *Mon. Wea. Rev.*, **100**, 518–541.

——, 1973: Temporal variation of low-latitude zonal circulations. *Mon. Wea. Rev.*, **101**, 803–816.

——, 1981: Mechanisms determining the mean and transient structure of the large-scale winter monsoon circulation. *Proc. Int. Conf. on Early Results of FGGE and Large-Scale Aspects of Its Monsoon Experiments*, Tallahassee, WMO, **4**, 20–29.

Williams, M., 1981: Interhemispheric interaction during Winter MONEX. *Proc. Int. Conf. on Early Results of FGGE and Large-Scale Aspects of Its Monsoon Experiments*, WMO, **10**, 12–16.